EFFECT OF THE INNER DIAMETER AND REYNOLDS NUMBER ON THE RECIRCULATION ZONE IN ANNULAR JET FLOW

MEROUANE HABIB[*], SAHNOUN RACHID and DRAI ISMAIL
Department of Mechanical Engineering, Faculty of Science and Technology
University of Mascara, ALGERIA
E-mail: mer_habib@yahoo.fr

In this paper, we focus on the effect of the inner diameter and Reynolds number on the recirculation zone in an annular jet flow with numerical simulation by resolving the Reynolds-averaged Navier-Stokes equations with the first closed model of turbulence k-epsilon. The annular jet plays an essential role in stabilizing the flame in the burner which is used in many industrial applications. The annular jet is characterized by the inner and outer diameter. In this study, three different inner diameters are adopted with constant width of the annular jet. We adopted also three different values of the Reynolds number show the effect of the Reynolds number on the recirculation zone. The simulation is realized by a CFD code which uses the finite element method. The results obtained from this study are in good agreement with the experimental data. Two recirculation zones are shown; a large recirculation zone at the outlet of the flow and a small recirculation zone just near the injection generated by the annular flow and the inner diameter D_i; it is observed that the size of the recirculation zone increases when the inner diameter increases and the length of the recirculation zone depends only on the inner diameter. This recirculation zone is also affected by the Reynolds number with a very low variation of the recirculation length.

Keywords: jet flow, annular jet, recirculation zone.

1. Introduction

Annular jets are usually encountered in many applications such as propulsion of rockets, combustion engines, gas turbine, etc). The annular jet is formed by obstacles placed in the inner jet called bluff body, it is characterized by the inner and outer diameter, this shape generates a central recirculation zone in the near-field which gives a good mixing for combustion, stabilizing flame and reducing pollutant emissions such as NOx. The annular jet flow is characterized by the diameter ratio D_i / D_o, where D_i is the inner diameter and D_e the outer diameter. Several researchers have divided annular jets into three zones, the initial zone, a transition zone and finally a fully developed jet zone [1-4].

Many experimental and numerical research works have been published on the annular jets flow, for example: Sheen *et al.* [5], Vanierschot and Bulck [6], Patte-Rouland *et al.* [7], Moore *et al.* [8], Ko *et al.* [9], Boguslawski *et al.* [10], Zhang *et al.* [11], Percin *et al.* [12], Himadri Chattopadhyay [13], Yang *et al.* [14].

The experimentalists show that the reverse mass flow rate increases with increasing blockage ratio, at the same time as the vortex length decreases with increasing blockage ratio due to the decreasing ratio of inertia to pressure force. Moreover, an increased body angle (from the cylinder to the disk) leads to outward oriented streamlines and therefore to a longer and wider recirculation bubble, having again an increased reverse mass-flow rate. Behind the bluff-bodies high values of turbulent intensity were measured, which rapidly decay more downstream in the established flow region.

Philippov *et al.* [15] studied the annular jets by using laser Doppler Anemometry (LDA). The results obtained show a very large recirculation zone in the central part of the jet. The inner and outer surfaces of the

---

[*] To whom correspondence should be addressed

annular jet are characterized by low intensity of turbulence. For a non-swirling annular jet, the average velocity and velocity RMS establish two flow regions. The first characterizes a swirling vortex; the second presents a weakly turbulent flow.

Ryzhenkov and Mullyadzhanov [16] studied the laminar annular jet by using direct numerical simulations for two diameter ratios *0.5*, *0.9*. They found that the stagnation point moved relative to the jet axis with increasing diameter ratio and they observed the appearance of asymmetric states and unstable fluid for high Reynolds number.

Terekhov *et al.* [17] investigated the flow and heat transfer in an impinging annular and round jet by using the PIV-measurement. The results are obtained for the same mass flow and data as a round jet. They observed that under these conditions of comparison the values of speed and turbulent pulsations in the annular jet are significantly higher than in the case of a round jet. The heat transfer intensity of the impinging annular jet is also higher than in the round jet.

Wawrzak, Karol *et al.* [18] investigated numerically non-swirling annular jets with using large eddy simulations for various Reynolds numbers and shear layer thicknesses. They observed that both parameters affect the dynamics of the flow. Instantaneous flow fields reveal the formation of spiral structures located in the inner and outer mixing layers. The analysis also shows that the structures are the result of instability which leads to the precession of the recirculation region formed in the near field.

Arathi Laldinpuii Kurup *et al.* [19] studied the flow field of two aligned coaxial jets consisting of an inner primary jet and an outer jet; The two-component laser-doppler-velocimetry technique was used for measurements of mean velocities and Reynolds stresses. They found that in the region between the outlets of the two jets, a toroidal recirculation vortex forms due to gradients of opposing pressure. They also observed in the presence of transverse injection, the vortex forms in two regions with radials drifting flow structures which substantially increase the decay of axial speed and the propagation rate at twice the values with respect to the characteristics of the primary jet alone.

The objective of this work is to characterize and identify the behavior of an annular jet in a turbulent flow for different inner diameters and Reynolds number and to compare the numerical results with the experimental data. We investigate in this paper the effect of the inner diameter and Reynolds number at the recirculation zone of the annular jet flow by using the k-epsilon model. Three different inner diameters are adopted with constant width of the annular jet: a) $\left(D_i = 36.75\ mm\right)$; b) $\left(D_i = 48.75\ mm\right)$ and c) $\left(D_i = 60.75\ mm\right)$. We adopted also in this study three different values of the Reynolds number $Re = 2630$, *4932* and *9865* to show the effect of the Reynolds number at the recirculation zone. The averaged equations of Navier-Stokes are solved by the numerical method with the finite element method. The geometry of the computational domain is characterized by the inner and outer diameter, the area is modeled for *2D* dimensions with radius $H = 100mm$ and length $L = 200mm$. The results obtained in this study of the axial, radial mean velocities and turbulent kinetic energy are presented in profiles and contours forms. The predicted results are compared with experimental results available in the literature.

2. Mathematical modeling

An incompressible fluid is assumed in this study, and the flow is considered to be steady and symmetric.

2.1. Continuity equation

The continuity equation in the Cartesian coordinate system is written in following form:

$$\frac{\partial \overline{u}_i}{\partial x_i} = 0 \ .$$
(2.1)

2.2. Momentum equation

The momentum equation is written in following form:

$$\bar{u}_j \frac{\partial (\rho \bar{u}_i)}{\partial x_j} = -\frac{\partial \bar{p}}{\partial x_i} + g_i + \frac{\partial}{\partial x_j}\left(\bar{\tau}_{ij} - \rho \overline{u_i' u_j'}\right) \tag{2.2}$$

where $\bar{u}_i$ and $\bar{u}_j$ are the time-averaged velocity in the i and j direction, u_i' and u_j' are the fluctuation velocities, $\bar{p}$ is the mean pressure, ρ is the fluid density, $\bar{\tau}_{ij}$ is the mean viscous stress tensor of the mean viscosity, given by:

$$\bar{\tau}_{ij} = 2\mu \bar{S}_{ij} = \mu \left(\frac{\partial \bar{u}_i}{\partial x_j} + \frac{\partial \bar{u}_j}{\partial x_i}\right)_{ij}, \tag{2.3}$$

where $-\rho \overline{u_i' u_j'}$ is the Reynolds stress tensor.

2.3. Standard k-ε turbulence model

The standard $k-\varepsilon$ model is based on the Boussinesq theory, which assumes that the Reynolds stress is modeled linearly to mean rate of strain, directly equivalent to the relative viscosity.

$$-\rho \overline{u_i' u_j'} = \mu_t \left(\frac{\partial \bar{u}_i}{\partial x_j} + \frac{\partial \bar{u}_j}{\partial x_i}\right) - \frac{2}{3}\rho k \delta_{ij} \tag{2.4}$$

where k is the turbulent kinetic energy given by:

$$k = \frac{1}{2}\overline{u_i' u_i'}, \tag{2.5}$$

μ_t is the turbulent viscosity calculated by the combination of the turbulence kinetic energy k and its dissipative rate ε as follows:

$$\mu_t = \rho C_\mu \frac{k^2}{\varepsilon} \tag{2.6}$$

where ε is the dissipative rate computed as follows:

$$\varepsilon = \frac{\mu_t}{\rho}\left(\overline{\frac{\partial u_i}{\partial u_j} \frac{\partial u_i}{\partial u_j}}\right). \tag{2.7}$$

In the standard $k-\varepsilon$ model the eddy viscosity has two unknown variables k and ε. It is necessary to provide the transport equations for k and ε derived from the momentum equation as follows:

$$\frac{\partial}{\partial t}(\rho k) + \frac{\partial}{\partial x_i}(\rho k \bar{u}_i) = \frac{\partial}{\partial x_j}\left[\left(\mu + \frac{\mu_t}{\sigma_k}\right)\frac{\partial k}{\partial x_j}\right] + G_k + G_b - \rho\varepsilon - Y_M + S_k \,, \tag{2.8}$$

$$\frac{\partial}{\partial t}(\rho\varepsilon) + \frac{\partial}{\partial x_i}(\rho\varepsilon\bar{u}_i) = \frac{\partial}{\partial x_j}\left[\left(\mu + \frac{\mu_t}{\sigma_\varepsilon}\right)\frac{\partial\varepsilon}{\partial x_j}\right] + C_{\varepsilon1}\frac{\varepsilon}{k}(G_k + C_{\varepsilon3}G_b) - C_{\varepsilon2}\rho\frac{\varepsilon^2}{k} + S_\varepsilon \tag{2.9}$$

where G_k and G_b are the production of turbulence kinetic energy caused by the mean velocity gradients and buoyancy, respectively.

$$G_k = -\rho\overline{u_i'u_j'}\frac{\partial u_i}{\partial x_i} \,, \tag{2.10}$$

$$G_b = \beta g_i \frac{\mu_t}{\mathrm{Pr}_t}\frac{\partial T}{\partial x_i} \tag{2.11}$$

where β is the coefficient of the thermal expansion.
The constants for this model are given in Tab.1.

Table 1. Constants for the standard $k - \varepsilon$ model.

C_μ	$C_{\varepsilon1}$	$C_{\varepsilon2}$	$C_{\varepsilon3}$	σ_k	σ_ε
0.09	*1.44*	*1.92*	*0.5*	*1.0*	*1.3*

3. Computational details

Figure 1 present the computational domain used to predict the turbulent flow in the annular jet. The schematic of the annular jet is characterized by the inner and outer diameter D_i and D_e, respectively. The width of the annular jet e is constant; three positions are adopted in this study.

The numerical method for this simulation is performed by using a CFD code which uses the finite element method and the k-epsilon model of turbulent to resolve the governing equations of the fluid flow.

Figure 2 shows the mesh generated by the CFD code with the fine and quadrilateral cells. The computational domain is modeled for dimensions *2D* of radius $H = 100mm$ and $L = 200 \ mm$ in length, the mesh is refined near the annular jet and the axis.
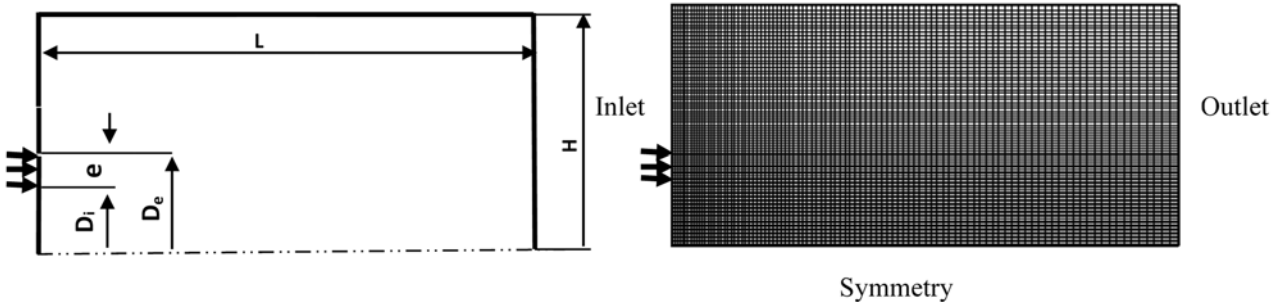

Fig.1. Schematic diagram of the computational domain.   Fig.2. Schematic of the computational grid.

4. Boundary conditions

Four faces boundary conditions are applied for the computational domain to predict the annular jet flow: the inlet air boundary, the wall boundary, the symmetry condition and the outlet air flow boundary. In the inlet air flow boundary a uniform velocity is adopted $U_0 = 8 \ m/s$; in the wall boundary a no-slip condition is applied.

5. Mesh test sensitivity

The mesh generated is composed of quadrilateral cells elements. Two different meshes are used to test the sensitivity of the numerical solution, the first mesh (grid 1) with *6560* nodes and the other mesh (grid 2) with *9920* nodes. The test of the two meshes is realized for the axial velocity in the axis symmetry (Fig.3) and compared to the experimental data. We adopt the refined mesh.
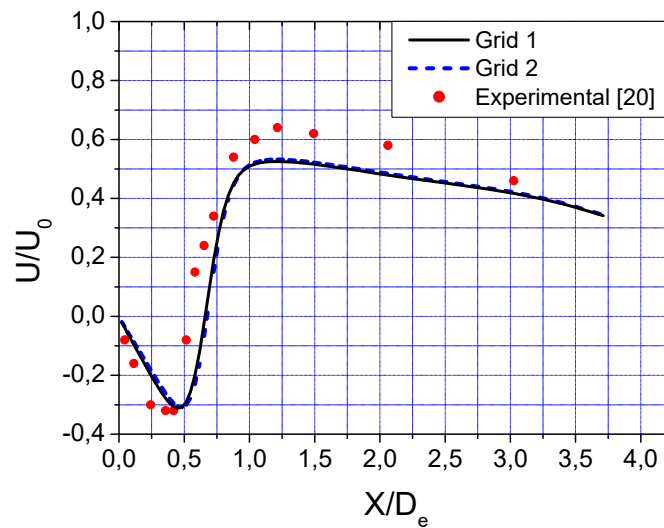
Fig.3. Mesh test sensitivity.

6. Results and discussion

In this study, we present a numerical simulation results obtained by the CFD code of the annular jet with three different inner diameters a) $(D_i = 36.75 \ mm)$; b) $(D_i = 48.75 \ mm)$ and c) $(D_i = 60.75 \ mm)$ The flow is considered asymmetric and two-dimensional; the governing equations are solved by the finite element method.

We present in the first section the view of the mean axial velocity and turbulent kinetic energy contour with three different inner diameters. To test and proof our first initial numerical simulation an experimental configuration is adopted to compare our results. The profiles of many quantities are plotted at different axial and radial positions, the mean axial and radial velocity are computed by the k-epsilon model and compared with the experimental data.

Figures 4 to 6 present the results of the mean axial velocity contours computed by the k-epsilon model for three different diameters $D_i = 36.75 \ mm$, $48.75 \ mm$ and $60.75 \ mm$. The width of the annular jet is constant but its position is variable in the radial axis. We observe in these figures the presence of two recirculation zones; a large recirculation zone at the outlet of the flow and a small recirculation zone just near the injection generated by the annular flow and the inner diameter D_i. It is noted that the recirculation zone depends essentially on the inner diameters D_i and on the outer diameter D_e or the position of the annular jet. It is

observed that the diameter of the recirculation zone increases when the inner diameter increases. We also notice the presence of two shear layers induced by the annular jet.

Figures 7 to 9 show the contours of the turbulent kinetic energy for the different diameters according to the displacement of the annular jet thickness. The results are obtained by the k-epsilon model; we observe a great dependence of the turbulent kinetic energy on the position of the annular jet thickness which increases significantly when the position of the annular jet thickness moves away from the jet axis. We observe also that the turbulent kinetic energy is concentrated in the recirculation region in the central zone of the flow near the jet and on the outside of the shear layer. The turbulent kinetic energy is quickly dissipated further downstream.
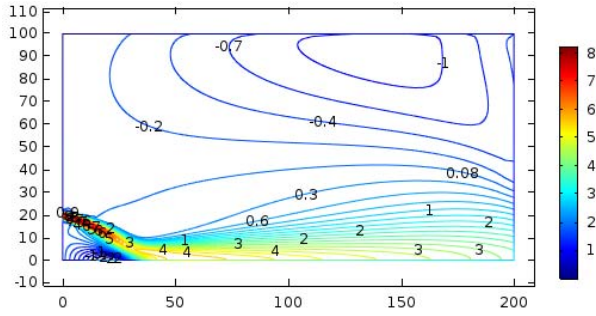
Fig.4. Axial mean velocity contour for $D_i = 36.75\ mm\ (m/s)$.
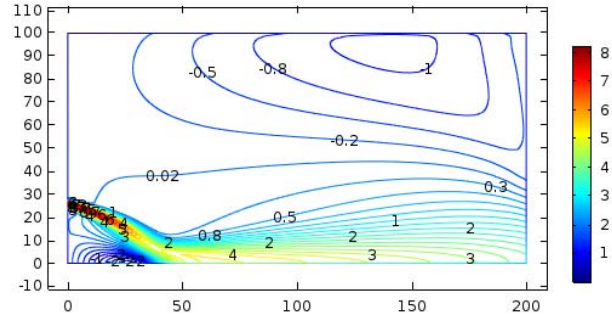
Fig.5. Axial mean velocity contour for $D_i = 48.75\ mm\ (m/s)$.
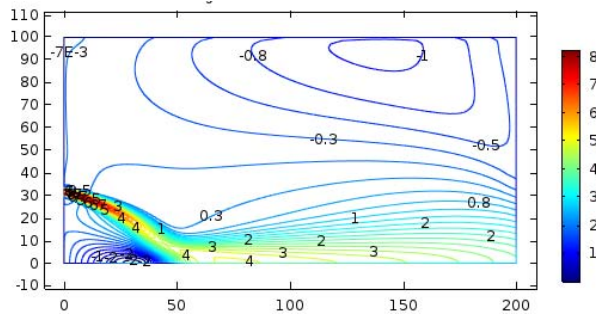
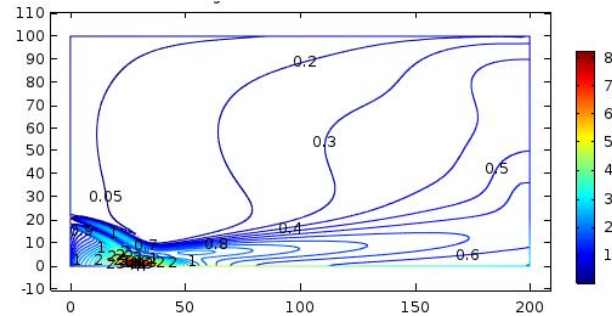Fig.6. Axial mean velocity contour for $D_i = 60.75\ mm\ (m/s)$.

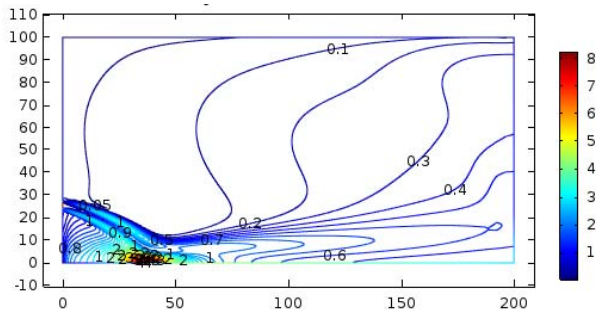Fig.7. Turbulent kinetic energy contours for $D_i = 36.75\ mm\ (m^2/s^2)$.

Fig.8. Turbulent kinetic energy contours for $D_i = 48.75\ mm\ (m^2/s^2)$.

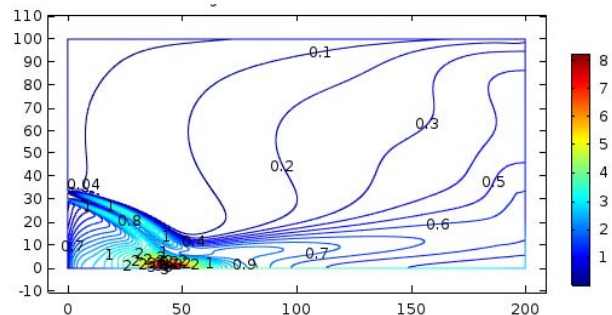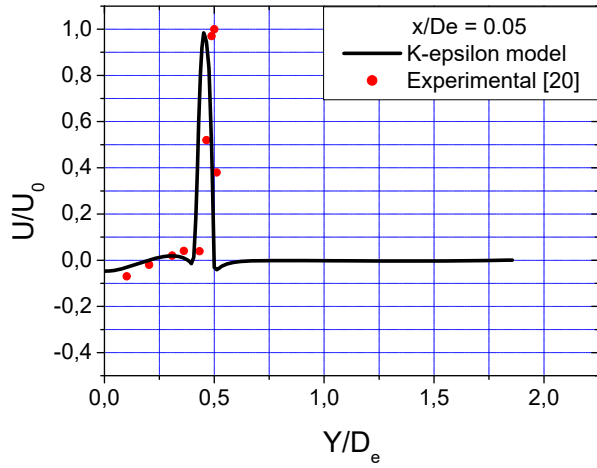Fig.9. Turbulent kinetic energy contours for $D_i = 60.75\ mm\ (m^2/s^2)$.

Fig.10. Axial velocity at $X / D_e = 0.05$.
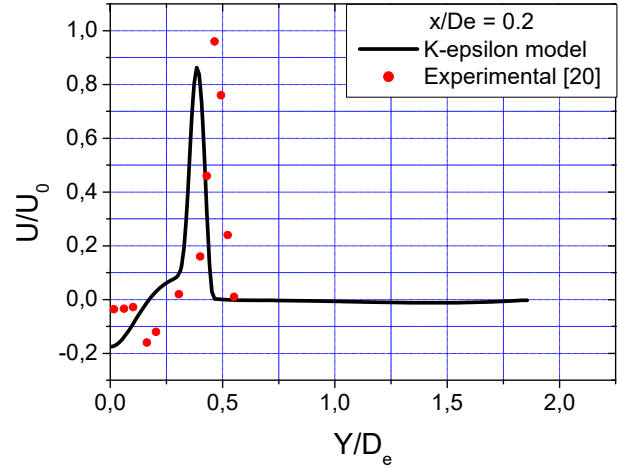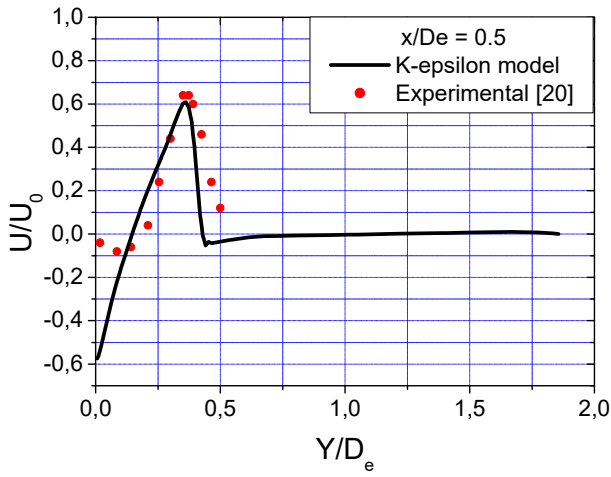

Fig.11. Axial velocity at $X / De = 0.2$.
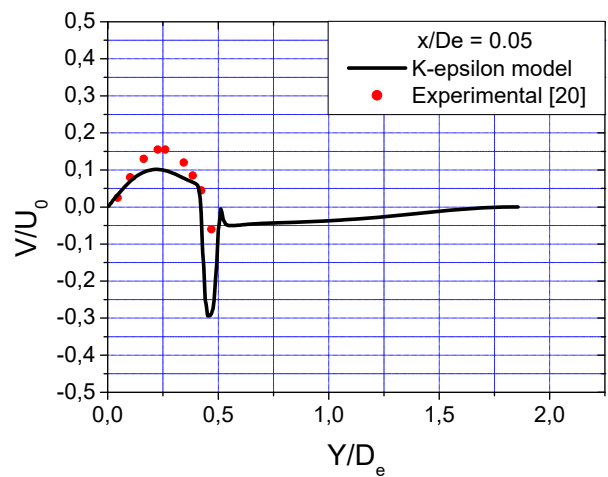

Fig.12. Axial velocity at $X / D_e = 0.5$.
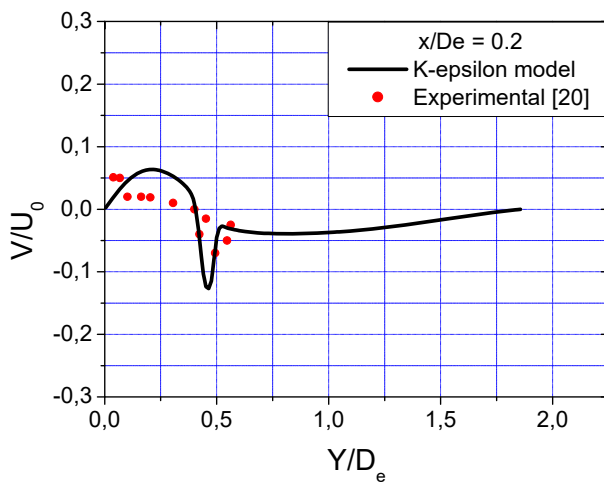

Fig.13. Radial velocity at $X / D_e = 0.05$.
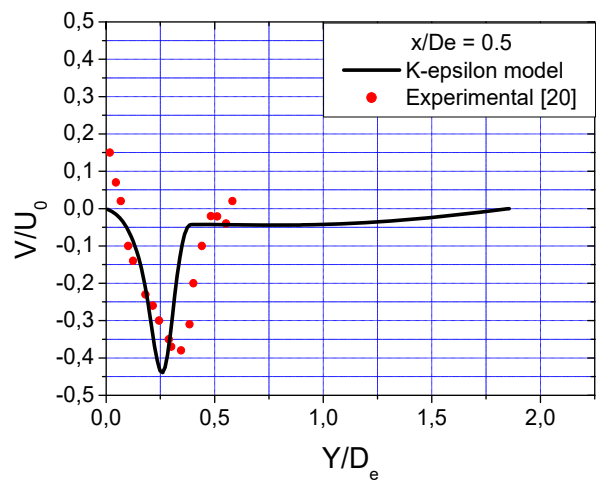

Fig.14. Radial velocity at $X / De = 0.2$.

Fig.15. Radial velocity at $X / De = 0.5$.

Figures 10, 11 and 12 show the profiles of the mean axial velocity obtained by the k-epsilon model at different axial positions $X / D_e = 0.05$, 0.2 and 0.5. The velocity profiles are negative in the vicinity of the jet axis at Y / D_e close to 0.2 due to the recirculation or reverse flow created by the bluff body of the annular jet. We observe in these figures the presence of a maximum peak created by the central of the jet flow. The peak velocity has a value around unity at the radial distance $Y / D_e = 0.47$ in position $X / D_e = 0.05$ and decreases gradually when the axial position increases. In general, the results obtained numerically by the k-epsilon model are in good agreement with the experimental data.

Figures 13, 14 and 15 illustrate the profiles of the mean radial velocity obtained numerically by the k-epsilon model at different axial positions $X / D_e = 0.05$, 0.2 and 0.5. In these figures the radial mean velocity is positive near the jet axis at Y / D_e less than 0.4 in location $X / D_e = 0.05$ and 0.2. We observe in these figures the presence of a negative peak in the opposite direction of the axial velocities profiles, the peak is important for the axial distance $X / D_e = 0.5$ and the maximum downward velocity is situated at $Y / D_e = 0.25$ with the value are about $-0.45\ U_0$. The k-epsilon model gives a good agreement with measurements data.
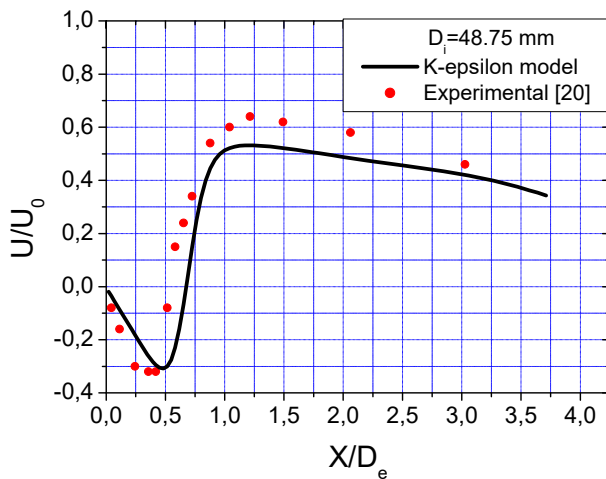

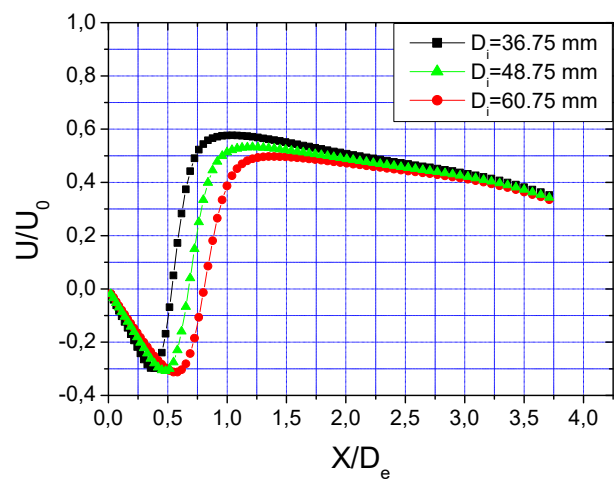Fig.16. Axial velocity in the symmetric axis compared with experimental data.

Fig.17. Axial velocity profiles for different inner diameters (m / s).

Figure 16 shows the profile of the mean axial velocity obtained at the symmetric of the axis. We observe in this figure a negative value of the axial velocity situated in the recirculation region near the jet axis. The profile is characterized by a negative peak of the axial velocity with a minimum value about $-0.3U_0$ at the position $X / D_e \sim 0.5$. The profile is also characterized by a stagnation point at the position $X / D_e \sim 0.6$ and the axial velocity becomes positive further downstream. The k-epsilon model gives a good agreement with measurements data.

Figure 17 shows the profile of the mean axial velocity at the symmetric of the axis for three different inner diameters $D_i = 36.75mm$, $48.75\ mm$ and $60.75mm$. This figure confirms the observation of the results shown in Figs 4, 5 and 6 of the mean axial velocity contours. It is noted that the recirculation length depends essentially on the inner diameters D_i and on the outer diameter D_e which increases when the inner diameter increases.

Figure 18 shows the profile of the mean axial velocity at the symmetric of the axis for different values of the Reynolds number $Re = 2630$, $Re = 4932$ and $Re = 9865$. We observe in this figure a small variation in the size of the recirculation zone when the Reynolds number is varied. The length of this zone increases appreciably when the velocity of the flow increases so we can say that the variation of the Reynolds number has a very small effect on the recirculation zone.

Figure 19 shows the results of the turbulent kinetic energy profiles at different axial locations $X / D_e = 0.05$, 0.2, 0.5, 1.5 and 3. The turbulent kinetic energy represents two oscillations or two peaks produced by the turbulent annular jet at $X / D_e = 0.05$ and 0.2. The first peak is caused by the core flow and central recirculation, the other peak is caused by the core flow and background co-flow. We observe also in this figure the profile of the turbulent kinetic energy. It is high near the jet axis at $X / D_e = 0.5$ and decreases further downstream.
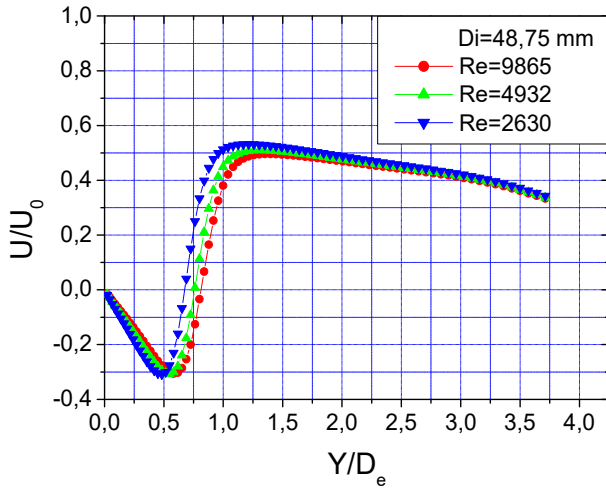

Fig.18. Axial velocity profiles for different values of the Reynolds number.
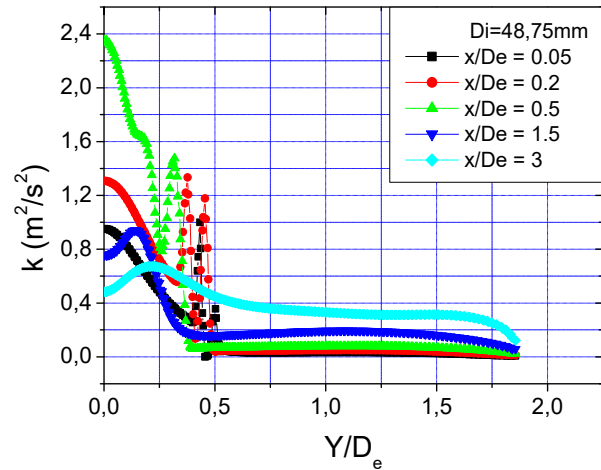
Fig.19. Turbulent kinetic energy profiles at different axial position $\left(m^2 / s^2 \right)$.

7. Conclusion

We present in this work a numerical study of an annular jet flow for three different inner diameters a) $\left(D_i = 36.75 \ mm \right)$; b) $\left(D_i = 48.75 \ mm \right)$ and c) $\left(D_i = 60.75 \ mm \right)$ with constant width of the annular jet. We present also the effect of the Reynolds number on the recirculation zone. Three different Reynolds number are adopted $Re = 2630$, 4932 and 9865. In this study, the first test of medium diameter is investigated numerically by the k-epsilon model and compared to the experimental data found in literature. The results obtained numerically show a good agreement with the experimental data. The results show two recirculation zones; a large recirculation zone near the outlet of the flow and a small recirculation zone just near the injection generated by the annular flow and the inner diameter D_i. It is observed that the diameter of the recirculation zone increases when the inner diameter increases and the length of the recirculation zone depends only on the inner diameter. This recirculation zone is also affected by the Reynolds number with a very low variation of the recirculation length. The turbulent kinetic energy decreases when the inner and outer diameter decrease and it is concentrated in the recirculation zone in the central region of the flow and shear layer.

Nomenclature

G — turbulence kinetic energy production

k — turbulent kinetic energy

P — mean pressure

u — mean velocity

u_i' — fluctuation velocity in i direction

u'_j − fluctuation velocity in j direction

β − thermal expansion coefficient

ε − dissipative rate

μ_t − turbulent viscosity

ρ − fluid density

$\overline{\tau}_{ij}$ − mean viscous stress tensor

References

[1] Vanierschot M. and Van den Bulck E. (2008): *Influence of swirl on the initial merging zone of a turbulent annular jet.*– Physics of Fluids, vol.20, 105104, doi:10.1063/1.2992191.

[2] Martins F.J.W.A., Kirchmann J., Kronenburg A. and Beyrau F. (2020): *Experimental investigation of axisymmetric, turbulent, annular jets discharged through the nozzle of the SPP1980 Spray Synburner under isothermal and reacting conditions.*– Experimental Thermal and Fluid Science, vol.114, 110052, doi:10.1016/j.expthermflusci.2020.110052.

[3] Del Taglia C., Blum L., Gass J., Ventikos Y. and Poulikakos. D. (2004): *Hysteresis in flow patterns in annular swirling jets.*– ASME.J. Fluids Eng., vol.126, No.3, pp.375-384.

[4] Danlos A., Lalizel G. and Patte-Rouland B. (2013): *Experimental characterization of the initial zone of an annular jet with a very large diameter ratio.*– Experiments in Fluids, p.32, 10.1007/s00348-012-1418-x.

[5] Sheen HJ., Chen WJ. and Jeng SY. (1996): *Recirculation zones of unconfined and confined annular swirling jets.*– AIAA Journal, vol.34, No.3, doi:10.2514/3.13106.

[6] Vanierschot M. and Van den Bulck E. (2007): *Hysteresis in flow patterns in annular swirling jets.*– Experimental Thermal and Fluid Science, vol.31, pp.513-524.

[7] Patte-Rouland B., Lalize G., Morea J. and Rouland E. (2001): *Flow analysis of an annular jet by particle image velocimetry and proper orthogonal de composition.*– Meas. Sci. Technol, vol.12, pp.1404-1412.

[8] Moore E.M., Shambaugh R.L. and Papavassiliou D.V. (2004): *Analysis of isothermal annular jets: comparison of computational fluid dynamics and experimental data.*– Journal of Applied Polymer Science, vol.94, pp.909-922.

[9] Ko N.W.M., Lau K.K. and Lam K.M. (1998): *Dynamics of interaction modes in excited annular jets.*– Experimental Thermal and Fluid Science, vol.17, Issue 4, pp.319-338.

[10] Boguslawski A. and Wawrzak K. (2020): *Absolute instability of an annular jet: local stability analysis.*– Meccanica, vol.55, pp.2179-2198.

[11] Zhang Y. and Vanierschot M. (2021): *Proper orthogonal decomposition analysis of coherent motions in a turbulent annular jet.*– Appl. Math. Mech.Engl. Ed, vol.42, pp.1297-1310, doi:10.1007/s10483-021-2764-8.

[12] Percin M., Vanierschot M. and Oudheusden, B.W.van (2017): *Analysis of the pressure fields in a swirling annular jet flow.*– Experiments in Fluids, vol.58, p.13, doi:10.1007/s00348-017-2446-3.

[13] Chattopadhyay H. (2004): *Numerical investigations of heat transfer from impinging annular jet.*– International Journal of Heat and Mass Transfer, vol.47, No.14-16, pp.3197-3201.

[14] Yang H.Q., Kim T., Lu T.J. and Ichimiya K. (2010): *Flow structure, wall pressure and heat transfer characteristics of impinging annular jet with/without steady swirling.*– International Journal of Heat and Mass Transfer, vol.53, No.19-20, pp.4092-4100.

[15] Philippov M.V., Chokhar I A, Terekhov V.V. and Terekhov V.I. (2020): *Flow evolution in the near field of a turbulent annular jet.*– Journal of Physics: Conference Series, vol.1565, Article Number 012070, doi:10.1088/1742-6596/1565/1/012070

[16] Ryzhenkov V.O. and Mullyadzhanov R.I. (2020): *Symmetry breaking in annular jets with different blockage ratio.*– Journal of Physics: Conference Series, vol.1677, Article Number 012028, p.6, doi:10.1088/1742-6596/1677/1/012028.

[17] Terekhov V.I., Kalinina S.V. and Sharov K.A. (2016): *An experimental investigation of flow structure and heat transfer in an impinging annular jet.*– International Communications in Heat and Mass Transfer, vol.79, pp.89-97.

[18] Wawrzak K., Boguslawski A., Tyliszczak A. and Saczek M. (2019): *LES Study of global instability in annular jets.*– International Journal of Heat and Fluid Flow, vol.79, 108460, doi:10.1016/j.ijheatfluidflow.2019.108460.

[19] Kurup A.L., Ölçmen S.M. and Anwar A. (2015): *Experimental study of co-annular jet subjected to transverse disturbances.*– Experimental Thermal and Fluid Science, vol.66, pp.53-62.

[20] Lalizel G. (2004): *Experimental characterization of the aerodynamics of an annular jet with a very large diameter ratio. Fluid dynamics.*– Phd thesis, University of Rouen.